POLITECNICO DI TORINO
Repository ISTITUZIONALE

Robust design methodologies to engineer multimaterial and multiscale bioprinters

Original
Robust design methodologies to engineer multimaterial and multiscale bioprinters / Bonatti, A.F., Batoni, E., Fortunato, G.M., Vitale-Brovarone, C., Vozzi, G., De Maria, C.. - In: BIOPRINTING. - ISSN 2405-8866. - 44:(2024). [10.1016/j.bprint.2024.e00372]

Availability:
This version is available at: 11583/2995014 since: 2024-12-04T18:09:41Z

Publisher:
Elsevier

Published
DOI:10.1016/j.bprint.2024.e00372

Terms of use:

This article is made available under terms and conditions as specified in the corresponding bibliographic description in the repository

Publisher copyright

(Article begins on next page)

18 November 2026

Bioprinting 44 (2024) e00372

Contents lists available at ScienceDirect

Bioprinting

journal homepage: www.sciencedirect.com/journal/bioprinting

Robust design methodologies to engineer multimaterial and multiscale bioprinters

Amedeo Franco Bonatti [a], Elisa Batoni [a,b], Gabriele Maria Fortunato [a,b], Chiara Vitale-Brovarone [c], Giovanni Vozzi [a,b], Carmelo De Maria [a,b,*]

[a] *Research Center "E. Piaggio", University of Pisa, Pisa, Italy*
[b] *Department of Information Engineering, University of Pisa, Pisa, Italy*
[c] *Department of Applied Science and Technology, Politecnico di Torino, Turin, Italy*

ARTICLE INFO

Keywords:
Multimaterial and multiscale bioprinting
Custom hardware and software
Robust engineering methodologies
LinuxCNC

ABSTRACT

Commonly used bioprinting technologies (e.g., material extrusion, material jetting) enable the fabrication of complex, multimaterial and multiscale scaffolds with controlled properties for tissue engineering applications. This enables the fabrication of scaffolds that more accurately replicate the structure of natural tissues. Despite the availability of commercial bioprinters, their high cost and lack of customization have driven researchers to modify existing devices or create entirely new platforms. Among all the available examples in literature, there is a strong need for more modular systems which are robustly designed taking into consideration the specific needs of bioprinting. In this context, the aim of this work is to introduce robust engineering methodologies to design and fabricate custom hardware and software for multimaterial and multiscale bioprinting. Firstly, we will identify the main design requirements that should be considered for a bioprinter (e.g., encumbrance, positioning resolution). Based on these requirements, we will then propose an analysis of the key building blocks of a bioprinter, including hardware (i.e., positioning system, toolheads, additional modules for extended functionalities), electronics (i.e., power supply, control boards), and software, introducing for each one the main concepts and equations for its optimal design. Throughout the work, we will use a customized bioprinting platform (namely, the BOOST bioprinter) as an example of the application of the proposed methodologies. Finally, we will present a validation of the methodologies and the bioprinter by fabricating high quality scaffolds through the combination of material extrusion and material jetting. The firmware developed during this work is available online as a support for developing more robust customized bioprinters.

1. Introduction

In the context of Tissue Engineering (TE), bioprinting has been defined as the use of Additive Manufacturing (AM) technologies as a bottom-up approach to fabricate scaffold-based constructs for TE applications, including implantation and *in vitro* modelling [1]. Currently, bioprinting techniques can be used to print both bioinks (i.e., inks containing cells with or without the addition of one or more supporting biomaterials) and biomaterial inks (i.e., inks containing only biomaterials). In the latter case, the scaffolding structure is printed first, and seeded with cells in a second, separate step [2]. The number and variety of AM techniques that can be used to process biomaterial inks is greater than those for bioinks, as there are no strict requirements related to cell damage that may exclude a processing technique (e.g., use of high temperatures, damaging shear stress) [3]. In the bioprinting literature, multiple technologies have been proposed for biomaterial ink scaffold fabrication, among which extrusion-based bioprinting (EBB), fused deposition modelling (FDM, known also as Fused Filament Fabrication), and inkjet bioprinting (IJB) rank among the most used ones [4]. In EBB, the material, usually a hydrogel contained in a syringe, is deposited layer-by-layer onto a printing plate by applying a pressure either through pneumatic or mechanical actuation on the syringe plunger [5]. EBB can process a wide variety of materials, with a viscosity up to 10^4 Pa*s, uses simple hardware and is easy to operate [6], and as a result has been applied successfully to fabricate constructs for the regeneration/modelling of different tissues such as bone [7,8] and cartilage [9,10]. FDM is an AM technique which can be used to produce scaffolds using rigid thermoplastic materials, usually provided in form of filament

* Corresponding author. Department of Information Engineering, University of Pisa, Pisa, Italy.
E-mail address: carmelo.demaria@unipi.it (C. De Maria).

https://doi.org/10.1016/j.bprint.2024.e00372
Received 15 May 2024; Received in revised form 18 November 2024; Accepted 19 November 2024
Available online 23 November 2024
2405-8866/© 2024 The Authors. Published by Elsevier B.V. This is an open access article under the CC BY license (http://creativecommons.org/licenses/by/4.0/).

Table 1
Summary of the main solutions for custom bioprinters developed by researchers, with technical details related to their design and fabrication.

Modified printer	# of compatible printing technologies	Type of printing technologies	Modularity	Software toolchain	Year	Ref
Flashforge Finder	1	EBB (single extruder)	–	Firmware: RepRap Slicer: Slic3r (Prusa Edition)	2022	[21]
Ender 3 Pro	1	EBB (dual extruder)	–	Firmware: Marlin-based Slicer: Slic3r (Prusa Edition)	2022	[23]
Prusa i3	1	EBB (single extruder)	–	Firmware: Marlin Slicer: Slic3r (Prusa Edition)	2019	[24]
Creality Ender 3 V2	1	EBB (single extruder)	–	Firmware: Marlin Slicer: Cura	2024	[26]
Prusa i3	2	EBB (single extruder) + FDM	Yes, syringe adapters for heating EBB	Firmware: Marlin Slicer: Slic3r (Prusa Edition)	2021	[27]
E3D tool changer motion system	1	EBB (dual extruder)	–	Firmware: RepRap Slicer: Simplify3D	2021	[28]
BCN3D+ Witbox2 Sigma	1	EBB (single extruder)	Yes, modular design of the printhead to use differently sized syringes, temperature-controlled extruder	Firmware: NA Slicer: NA	2020	[29]
Geetech Pro i3	1	EBB (single extruder with millifluidic mixing unit)	–	Firmware: Marlin Slicer:	2024	[30]
Custom	3	EBB + FDM + electrohydrodynamic printing	Yes, toolheads can be switched using a custom toolchanger mechanism	Firmware: Slicer:	2022	[34]
Prusa i3	1	EBB + FDM	Yes, allowing switching between EBB and FDM	Firmware: Prusa firmware Slicer: Slic3r	2021	[35]
Custom	2	EBB + electrohydrodynamic printing processes	–	Firmware: NA Slicer: NA	2021	[36]
Custom	1	EBB (multiple extruders)	Yes, temperature-controlled extruder	Firmware: Marlin Slicer: Cura	2017	[37]
Custom	1	EBB (single extruder, coaxial configuration) + IJB	Yes, temperature-controlled extruder	Firmware: Marlin Slicer: Slic3r	2019	[39]
Voron 0.1	2	FDM (filament and pellet extrusion) + Melt electrowriting	–	Firmware: Slicer:	2023	[40]
Custom	3	EBB + FDM + IJB	Yes, toolheads can be switched thanks to a custom toolchanger mechanism	Firmware: Marlin	2024	[41]

but also in more niche applications directly as pellets. When compared to pellet feedstock, filaments allow for a more homogeneous product at the cost of increased production time (as the process becomes a two-step one, first obtaining the filament from pellets and then printing) and increased risk of thermal degradation depending on the polymer to be processed [11,12]. In FDM, the material passes in a hot region to facilitate its extrusion through a printing nozzle and deposited onto the plate. In the context of bioprinting, FDM has been mainly adopted in fabricating scaffolds for rigid tissue engineering like bone [13–15]. Finally, inkjet bioprinting (IJB) is commonly used to directly print cells [16,17] or to locally deposit biological material in precise positions on the surface/inside a bioprinted scaffold [18]. The common IJB set-up consists of a cartridge, which contains the material to be printed, and the nozzles through which the ink drop is ejected. The mechanism of droplet formation varies depending on the IJB technique. For example, in thermal drop-on-demand (DOD) inkjet, the acqueous material is heated at high temperature to create a bubble, which in turn pushes the material out of the nozzle. On the other hand, in piezoelectric DOD inkjet a voltage pulse (with precise amplitude and temporization) is applied to a piezoelectric element which deforms and produces a pressure wave that enables the jetting process [19].

Although bioprinter commercialization represent an important share of the bioprinting market [4,20], several groups have reported the development of custom bioprinters/toolheads as alternative, more customizable, and cheaper solutions to commercial hardware [21–26], as summarized in Table 1. For instance, Koch et al. showed the open-source modification of a commercial Prusa i3 FDM 3D printer with the inclusion of a syringe pump for EBB. The authors fabricated a proof-of-concept composite scaffold for bone TE applications by continuously alternating between a rigid, FDM-printed PCL support and an extrusion-bioprinted gelatin-alginate hydrogel [27]. Similarly, Engberg et al. modified the commercial E3D tool-changer system to include a mechanical syringe extruder for bioprinting applications. The tool-changer system enables the easy integration of multiple extruders to obtain multimaterial scaffolds with high resolution. To validate the platform, the authors printed a collagen biomaterial ink alongside a cell-laden laminin bioink inside a supporting bath (namely, FRESH bioprinting technique) [28]. Sanz-Garcia et al. presented the design and implementation of a custom toolhead for EBB with a temperature control in the range 2–60 °C. The toolhead versatility was validated by mounting it on three different open-source 3D printers, demonstrating its potential as a low-cost replacement of commercial solutions [29]. Finally, Mohammadi et al. have very recently proposed the MOS3S (Microfluidic Open-Source 3D bioprinting system) platform, consisting in the modification of a Prusa i3 machine with a microfluidic toolhead, to fabricate hierarchical scaffolds for TE applications. The microfluidic toolhead consists in multiple syringe extruders feeding the biomaterials at different rations towards a microfluidic chip, allowing to create gradient structures [30]. A current trend in bioprinting research is to combine multiple technologies together onto the same machine, enabling the fabrication of 3D structures able to recapitulate the complex multiscale architecture and composition of human native tissues/organs [31–33]. Several examples have been reported in literature on the development of customized multimaterial and multiscale bioprinters [34–37]. For example, Liu et al. developed an advanced cell printing platform by combining EBB with a droplet-based bioprinting technique

using a dual toolhead configuration. The EBB module was used to print strands of hydrogel materials containing a high cell density, while the jetting toolhead was used to print single cell containing droplets on the extruded filaments [38]. Similarly, Yenilmez et al. proposed a low-cost bioprinter which integrates both coaxial EBB and IJB together with a photocrosslinking tool-head. The authors validated their design by inkjet printing methacrylated gelatin (GelMA) together with extruded alginate [39]. Reizabal et al. modified an open source FDM printer to enable the melt-electrowriting process (i.e., an AM technique able to generate fibrous structures at micron scale resolution from a molten thermoplastic polymer by applying a high-voltage field) for bioprinting applications. The authors showed how the designed system could be used to produce multiscale, single material scaffolds by alternating FDM printing and melt-electrowriting in the same process. All files to replicate the design were made available so that other researchers could implement their own system [40]. Very recently, Phung et al. presented the development of a custom, cost-effective multi-head bioprinter to fabricate complex multimaterial and multiscale constructs. The bioprinter can operate two toolheads at a time and is compatible with screw-based FDM for direct pellet extrusion, co-axial extrusion, filament FDM and micro-valve printing [41].

Even though the previous examples highlight how different groups have developed their own bioprinting platform, there are still some limitations in the custom bioprinters landscape. Firstly, many bioprinters are conceived as modifications of already existing desktop 3D printers, for example by designing and fabricating additional toolheads. This is a major limitation because: i) the hardware is not tailored to the specific requirements of bioprinting (e.g., space constraints to work under a chemical/biological hood, protection of delicate components when printing with possibly damaging materials), ii) the modularity of the platform is limited, and additional plates/supports will be needed to integrate new printing toolheads or to add new functionalities to the printer. Furthermore, even for custom-designed platforms, robust engineering practices (i.e., a set of design methodologies that, if chosen from the beginning of the bioprinter development, will ensure achievement of targeted functionalities in a robust way) are not clearly presented, limiting the diffusion of these platforms to other laboratories and their adaption to new use-cases. In this context, the aim of this work is to present robust design methodologies to implement a custom bioprinting system from scratch with the final aim of producing scaffolds for TE applications. We will firstly present a comprehensive workflow to implement the bioprinter considering its main components (i.e., hardware, electronics, and software), and detail for each of them which are the main design choices to be made with the support of mathematical modelling. As an example application of these methodologies, the development of a custom bioprinter (termed the BOOST bioprinter [42]) will be also presented. The platform has already been used for the fabrication of high quality, repeatable scaffolds through EBB. Here, we will validate our design workflow by showing the functionality of the BOOST bioprinter for the fabrication of multimaterial and multiscale scaffolds using a combination of FDM and IJB and EBB and IJB. The firmware source codes are made available open source in a ZENODO repository (https://doi.org/10.5281/zenodo.10993098). STEP files of the bioprinter are available on request.

2. Materials and methods

2.1. Overview of the design workflow

Herein, we define a workflow to design a custom bioprinter able to fabricate multimaterial and multiscale scaffolds for TE applications. The workflow starts with the definition of the main design requirements that will guide the bioprinter development. These requirements are both quantitative (e.g., targeted values for positioning accuracy, precision, repeatability) and qualitative (e.g., compatibility of the software toolchain with standard software for AM) and will influence the development of the following steps. The latter focus on the three key building blocks of a bioprinter, namely the hardware, the electronics, and the software. The hardware encompasses all the physical components necessary to operate the printer, which mainly include the printing toolheads, the positioning system (which moves the printer end-effector in space), and any other additional module to increase the bioprinter functionality. Each hardware component is controlled though specific electronics modules, including for instance the power supply and the drivers for the toolheads and positioning system. Finally, a software layer is necessary to properly operate the bioprinter by orchestrating the movement of each hardware component controlled by the electronics. Overall, the union of all key building blocks enables the translation of the scaffold digital model into a physical product. Throughout the following sections, we will make use of the BOOST platform as an example of the application of this workflow to engineer a bioprinter. An overview of the CAD model for the BOOST bioprinting platform is reported in Fig. 1.

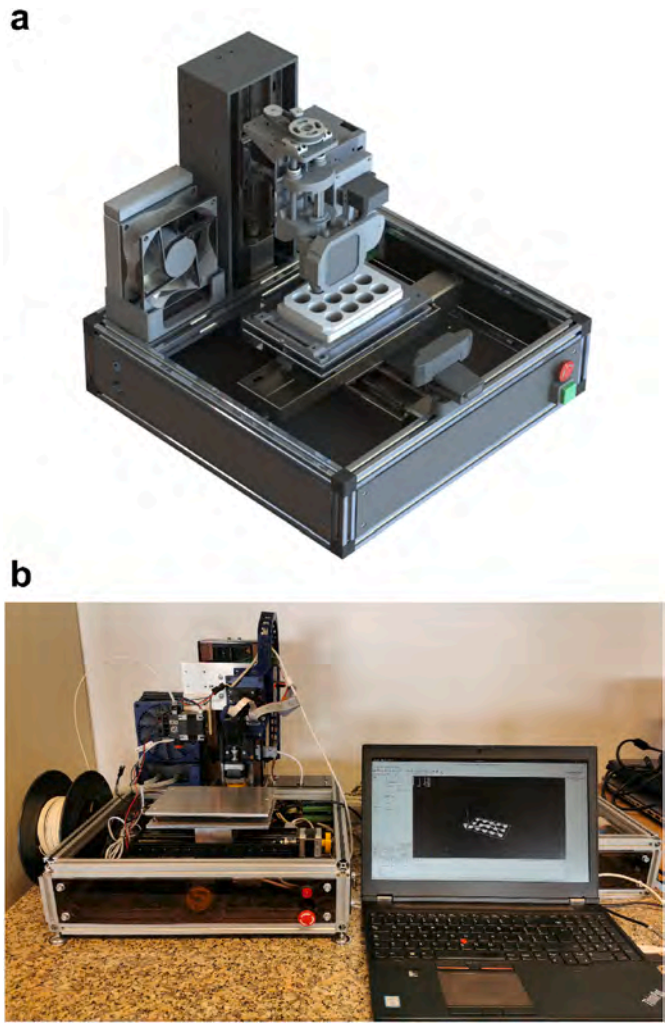


Fig. 1. In (a), the rendering of the CAD model of the BOOST bioprinting platform, while in (b) the fabricated platform.

2.2. Step 1: design requirements definition

Quantitative and qualitative requirements for the bioprinter should be clearly defined as the first step to design the platform, as they will directly control the development of the machine key building blocks. For instance, the decision on how many and which printing technologies should be implemented on the bioprinter will influence the design of the

Table 2
Summary of the main general design requirements to engineer a multiscale and multimaterial bioprinter.

Key design requirements to consider	Possible influence of the requirements on the building blocks
Type of printing technologies	• Hardware: the positioning system resolution, accuracy, and repeatability should be at least equal to the minimum resolution of all printing technologies. • Electronics: specific drivers should be implemented for each printing technology (e.g., stepper motor drivers for EBB and FDM, pulse generation electronics for IJB). • Software: relevant parameters for their operation should be set in the software (e.g., steps/mm parameter for EBB and FDM, excitation pulse temporization for IJB).
Number of printing technologies to be used at the same time	• Hardware: specific supports and a tool-changer mechanism should be implemented to allow multi-technology printing. The positioning system should accommodate multiple toolheads. • Electronics: the power supply should be able to output enough power to handle multiple toolheads operation at the same time. • Software: g-code solutions for multi-technology printing should be considered in the software implementation.
Overall weight and encumbrance	• Hardware: the overall weight and encumbrance may influence the choice of positioning system (e.g., the travel distance for each axis) and the number of compatible toolheads and additional modules.
Number and type of additional modules to be added	• Electronics: drivers for the additional modules should be included in the electronics. • Software: custom g-code commands should be implemented to integrate the modules operation in the printing process.
Compatibility with standard software toolchain	• Software: the chosen firmware should be compatible with standard g-code so that the printer can be operated with commonly used slicers.

overall supporting structure (in terms for example of weight constraints) and the selection of the positioning system (as the minimum feature resolution of the chosen printing technologies should be compatible with the resolution of the positioning system). A summary of key design requirements and how these may influence the building blocks development is reported in Table 2.

Taking into consideration the specific case of the BOOST bioprinter, the key requirements that guided its development included: i) compatibility with three deposition technologies, namely EBB, thermal IJB, and FDM, with the ability to use up to two in the same printing process. The choice of these specific printing technologies allows the bioprinter to process a wide variety of (bio)materials (i.e., thermoplastic polymer, hydrogels, pastes, liquid solutions) at two main length scales, namely below the millimetre one for EBB and FDM and below the hundreds of microns one for IJB. Accordingly, the targeted resolution (i.e., the smallest increment of motion that a positioning system is able to achieve), accuracy (i.e., the error between the measured position and the targeted one), and repeatability in positioning (i.e., the variation in actual positions after commanding the target position repeatedly under the same testing conditions) was chosen to be below the tens of microns range to enable the precise deposition of droplets through IJB. ii) small form factor and reduced weight so that the printer could fit inside a chemical/biological hood; iii) modularity of the platform, with the ability to expand it by adding new modules (e.g., new sensors, new controls on the toolhead and the environment); iv) increased control over the printing process, thanks to purposely designed toolheads.

2.3. Step 2: development of the hardware

The hardware building block represents the base of the bioprinting system. As previously highlighted, it is usually given by: i) the positioning system, ii) the printing toolheads, and iii) any additional modules.

2.3.1. Development of the positioning system

The positioning system should be able to move the printer end-effector (i.e., the toolheads) in space with a certain degree of accuracy, precision, and repeatability. The target values for these three parameters should be determined during the initial design requirements definition (see Section 2.1) and will influence the choice of the final positioning system.

In standard bioprinter hardware, a cartesian reference system is used, in which the position of the end-effector is specified relative to a X-Y-Z reference system. The end-effector movement is achieved using computer-controlled motors (typically stepper motors, although servo motors might also be used) either by moving the toolheads in the Z direction and the printing bed in the X and Y (namely, a bed-slinger system), or by moving the toolheads in the X and Y plane and the bed along the Z axis (namely, a Core-XY system). The main difference between a bed-slinger and a Core-XY resides in the mass to be moved during printing. In a Core-XY system, the toolheads are moving; this means that, for a single and lightweight toolhead, this configuration is inherently faster than a bed-slinger one, since in the latter the heavier printing bed will be the element to move. On the other hand, this also limits the number and weight of the mounted toolheads in a Core-XY system. When choosing a positioning system, it is thus important to consider its maximum load capacity F_{lc} (measured in [N]) and compare it with the mass to be moved. For instance, taking into consideration a bed-slinger system, the Z axis should be able to move the toolheads. If the toolheads have an overall mass $m_{toolheads}$ (measured in [kg]), F_{lc} should be thus greater than the weight force (Eq. (1)):

$$F_{lc} > m_{toolheads} \cdot g \tag{1}$$

Similarly, the X and Y axes should be able to move the mass of the bed m_{bed} (also measured in [kg]) and so we can write Eq. (2):

$$F_{lc} > m_{bed} \cdot g \tag{2}$$

Considering the specific case of the BOOST bioprinter, the positioning system is based on a cartesian, bed-slinger configuration using three stepper motor-actuated linear axes (VT-80, Physik Instrument). Specifically, the linear actuators corresponding to the X and Y axes move the bed while the vertical Z-axis moves the tool heads. In the BOOST bioprinter, the toolheads are attached to the Z axis by a custom-made support featuring a plate with threaded M4 holes used to fix multiple elements. The printing bed (composed by two rectangular plates with overall dimensions to fit a multiwell plate, separated by a spring-based three-point calibration system, as can be seen in Fig. 2b) is attached to the X axis, which in turn is mated to the linear actuator for the Y axis. Finally, the Z and Y axes are attached to a L-shaped support which was manufactured in house to guarantee that the two actuators are perpendicular one to the other (Fig. 2a).

The values for the moved mass and the resulting minimum load capacity for each axis is reported in Table S1, while relevant characteristics for the linear stages are presented in Table S2. Note that the X-axis has a higher travel range to accommodate multiple tool heads. The nominal resolution of the stages (5 μm) is compatible with the lowest resolution among the chosen printing technologies (see Section 2.2). Moreover, the high repeatability (±10 μm) in positioning enables the fabrication of scaffolds which are consistent across batches.

2.3.2. Development of the toolheads

Material extrusion (i.e., EBB, FDM) and jetting (i.e., IJB) rank among the most used bioprinting technologies in the field [4]. In the following

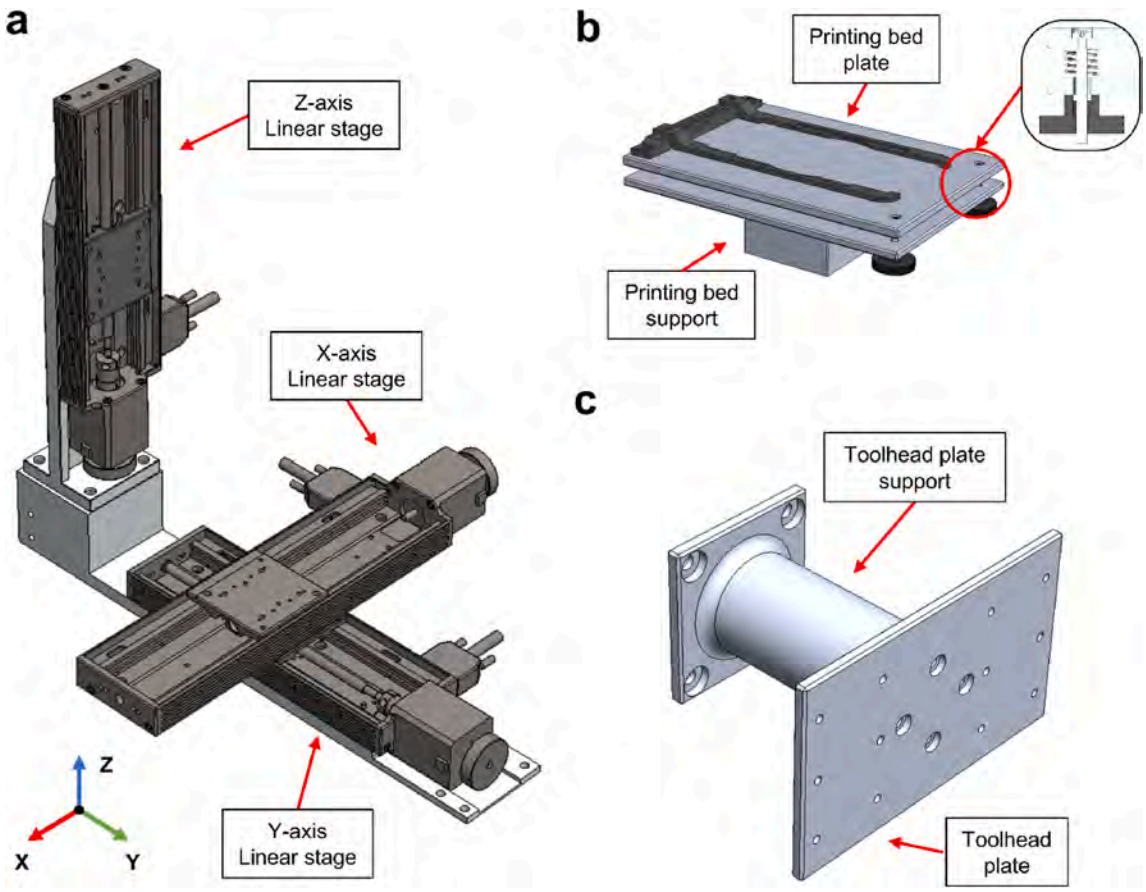


Fig. 2. Overview of the positioning system for the BOOST bioprinter: (a) the three stepper motor actuated linear stages in their mounting position; (b), an overview of the printing bed, which is attached to the X-axis linear stage; (c) an overview of the toolhead support, which is attached to the Z-axis linear stage.

sections, we will detail the design specifically of the mechanical extruder mounted on the BOOST bioprinter as an example on how to apply robust engineering methodologies for custom toolhead development. The FDM and IJB of the BOOST system are based on commercial solutions (REVO Hemera, E3D FDM extruder and Hewlett Packard C6602A cartridge and related support for the IJB toolhead, respectively) which were slightly adapted to be mounted on the toolhead support system (Fig. 3b and c). A tool-changer system was designed *ad hoc* to use two toolheads in the same printing process at any given time (Fig. 3d). Briefly, the system is based on a thrust-crank mechanism controlled by a servo motor, which moves up/down one of the attached toolhead to avoid any collision between the toolhead and the printing supports like petri dishes or multiwell plates. The down position corresponds to a mechanical stop to have a precise and repeatable position. A two-plates system enables quick and precise swapping between toolheads.

The CAD design for the piston-actuated extruder is illustrated in Fig. 3a. The extruder uses a NEMA 17 stepper motor (SY42STH47-1206B, SongYong hybrid stepper motor) to apply a force on the syringe plunger thus allowing material extrusion. The rotation of the motor shaft is transformed into a linear displacement of the plunger thanks to a composite transmission train with a belt-pulley mechanism in series with a M5 leadscrew one. Regarding the belt-pulley system, the input pulley is attached to the motor shaft through two M3 grub screws, while the output pulley is directly attached to the M5 leadscrew. As shown in Fig. 3a, the output pulley has a hexagonal slot for the head of a M5 self-locking nut, which is used for coupling the two elements. The lead screw is sustained by two flanged radial ball bearings, one attached to the top plate and one to the syringe support. Two self-locking nuts (one at the top, attached to the output pulley, and one at the bottom) keep the lead screw in place and transmit rotation to the ball bearings. With this solution, the rigidity of the extruder is increased since the extrusion force is decoupled from the motor and transmitted directly to the toolhead plate. Finally, the leadscrew is coupled to a carriage which applies the extrusion force to the syringe plunger (Fig. 3a). The coupling between these two elements is obtained through a hexagonal M5 long aluminum nut. Aluminum was chosen so that the nut will be the first element to wear compared to the steel leadscrew, allowing an easier and cheaper maintenance. The carriage vertical movement is constrained using two linear ball bearings (LM8UU) which slide on two 8 mm diameter steel rods. In a mechanical extruder, the main elements to consider in the design are that: i) the motor should be able to output enough torque at the required operating speed, and ii) the transmission mechanism should have a low inertia (i.e., the resistance of an object to change its angular velocity about an axis of rotation, measured in [kg•m^2]) to enable rapid changes in the extrusion speed during printing.

From a mathematical stand-point, we can analyse the BOOST extruder as a series of two transmission mechanisms, first the belt-pulley and then the leadscrew one. The transmission ratio for the belt-pulley mechanism N_{BP} (a-dimensional) is given by Eq. (3) [43]:

$$N_{BP} = \frac{\omega_{ip}}{\omega_{op}} = \frac{r_{op}}{r_{ip}} \tag{3}$$

here, ω_{ip} and ω_{op} refer to the angular velocity of the input (*i.e.*, the pulley connected to the motor shaft) and output pulley (*i.e.*, the pulley connected to the leadscrew) respectively (measured in [rad/s]), and r_{ip} and r_{op} to their radius (in [m]). The torque required by the motor T_m is related to the output torque of the belt-pulley mechanism T_{out}^{BP} (both in [N•m]) as (Eq. 4):

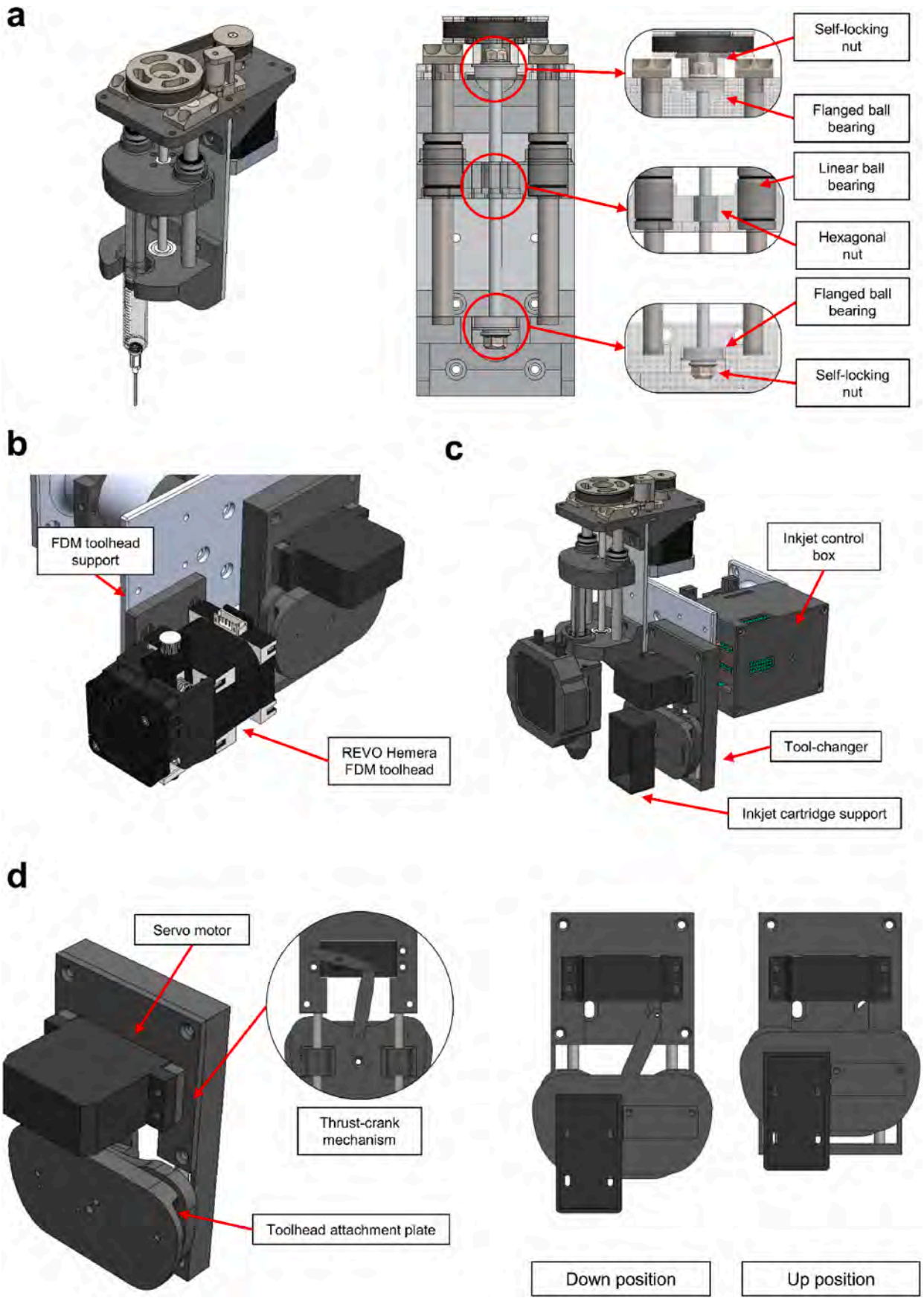


Fig. 3. Overview of the toolheads compatible with the BOOST bioprinter. In (a), a CAD visualization of the mechanical extruder and all its components. In (b), a CAD visualization of the FDM toolhead, while in (c) the inkjet toolhead mounted on the tool-changer mechanism. Finally, in (d) the toolchanger mechanism main components alongside the toolchanger two main positions (termed 'up' and 'down').

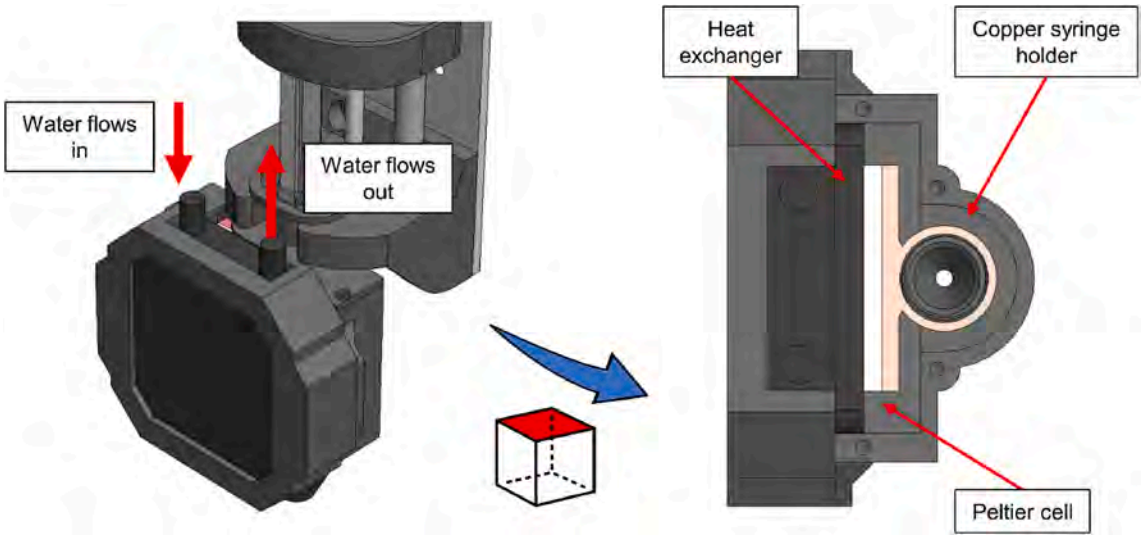


Fig. 4. overview of the water-based heat exchanger system for the Peltier heating/cooling system.

$$T_m = \frac{1}{\eta_{BP}} \cdot \frac{T_{out}^{BP}}{N_{BP}} \tag{4}$$

where η_{BP} is the efficiency of the belt-pulley mechanism (a-dimensional), which is lower than 1 due to friction effects. The reflected inertia at the motor shaft J_{ref}^{m} is given by the sum of the inertia of the input pulley J_{ip}, of the output pulley J_{op}, and of the load to be moved by the mechanism J_{load}^{BP} (Eq. (5)):

$$J_{ref}^{m} = J_{ip} + \frac{1}{\eta_{BP} N_{BP}^2} \left(J_{op} + J_{load}^{BP} \right) \tag{5}$$

All inertia terms are computed around the main axis of rotation of the element. Note that in Eq. (5) the belt inertia was not considered since it is low when compared to the other terms. To compute the inertia term of the two pulleys, an approximation to a hollow cylinder can be used: considering the outer radius r_{ext} and the inner radius of the cavity r_{int}, the height of the pulley H, and the density of the pulley material ρ (measured in [kg/m^3]), we can write the inertia term around the main axis of the cylinder as Eq. (6):

$$J_p = \frac{1}{2} m \left(r_{ext}^2 - r_{int}^2 \right) = \frac{\pi H \rho \left(r_{ext}^2 - r_{int}^2 \right)^2}{2} \tag{6}$$

A similar scheme can be followed for the leadscrew transmission, where the transmission ratio N_{LS} will be given by (Eq. (7)):

$$N_{LS} = \frac{\dot{\theta}_{LS}}{v_E} = \frac{2\pi}{p} \tag{7}$$

In Eq. (7), $\dot{\theta}_{LS}$ refers to the rotational speed of the screw (in [rad/s]) and v_E is the translational speed of the carriage coupled with the leadscrew. The parameter p is the pitch of the leadscrew (in [m/rev]) and as a result, N_{LS} is measured in [rev/m]. The torque is given by Eq. (8):

$$T_{in}^{LS} = \frac{F_{ext}}{\eta_{LS} N_{LS}} \tag{8}$$

where η_S is the efficiency of the transmission and F_{ext} is the force to be applied on the syringe plunger. Finally, the reflected inertia to the input of the leadscrew mechanism is given by Eq. (9):

$$J_{ref}^{LS} = J_{screw} + \frac{1}{\eta_{LS} N_{LS}^2} \left(F_{ext} + \frac{W_c}{g} \right) \tag{9}$$

here, W_c is the mass of the carriage (in [kg]) and g is the gravity acceleration (in [m/s^2]). The inertia J_{screw} can be found by approximating the leadscrew to a cylinder (Eq. (10)):

$$J_{screw} = \frac{1}{2} m r^2 = \frac{\pi L \rho D^4}{32} \tag{10}$$

where ρ is the density of the screw material, D is the diameter, and L is its length (both in [m]). Since the two mechanisms are used in series, $J_{load}^{BP} = J_{ref}^{LS}$ and $T_{out}^{BP} = T_{in}^{LS}$, and so Eq. (8) and Eq. (9) can be combined respectively with Eq. (4) and Eq. (5) to obtain the final relationship for J_{ref}^{m} and T_m.

To obtain smooth acceleration and deceleration profiles, the inertia ratio IR should be computed, as in Eq. (11):

$$IR = \frac{J_{ref}^{m}}{J_m} \tag{11}$$

J_m represents the inertia of the stepper motor rotor, listed in its datasheet. As a general rule of thumb, the inertia ratio should be lower than 10 [43]. Finally, T_m is the torque that the motor should supply to maintain extrusion at constant velocity. When doing accelerations, a term related to the torque necessary to move the whole transmission train should be added. If the required motor shaft angular acceleration is $\ddot{\theta}_m$, we can write Eq. (12):

$$T_{acc} = T_m + \ddot{\theta}_m J_{tot} \tag{12}$$

More details on the values used for each term of the previously described equations as well as the results for the analysis can be found in Table S3. Note that the efficiency for the leadscrew mechanism may vary between 35 and 85 %, while higher values can be considered for the belt-pulley one (90–99 %) [43]. Here, we used a value of 60 % for the efficiency of both mechanisms as a worst-case scenario considering that several components of the extruder for the BOOST bioprinter are obtained through 3D printing (e.g., the pulleys, the belt tensioner), thus errors may be introduced by the manufacturing process (e.g., alignment errors between components, less rigid and less dense components compared to metal parts) that can lower the overall efficiency. According to the table, the inertia ratio is around 10 so that the motor can accelerate and decelerate the transmission. Furthermore, the torque requirements (both at steady operation and during acceleration) are satisfied since, at the maximum speed and considering the precautionary extrusion load, the stepper motor can output around 0.15 N m (according to the torque-speed curves in the motor datasheet) which is well above both the computed T_m and T_{acc}.

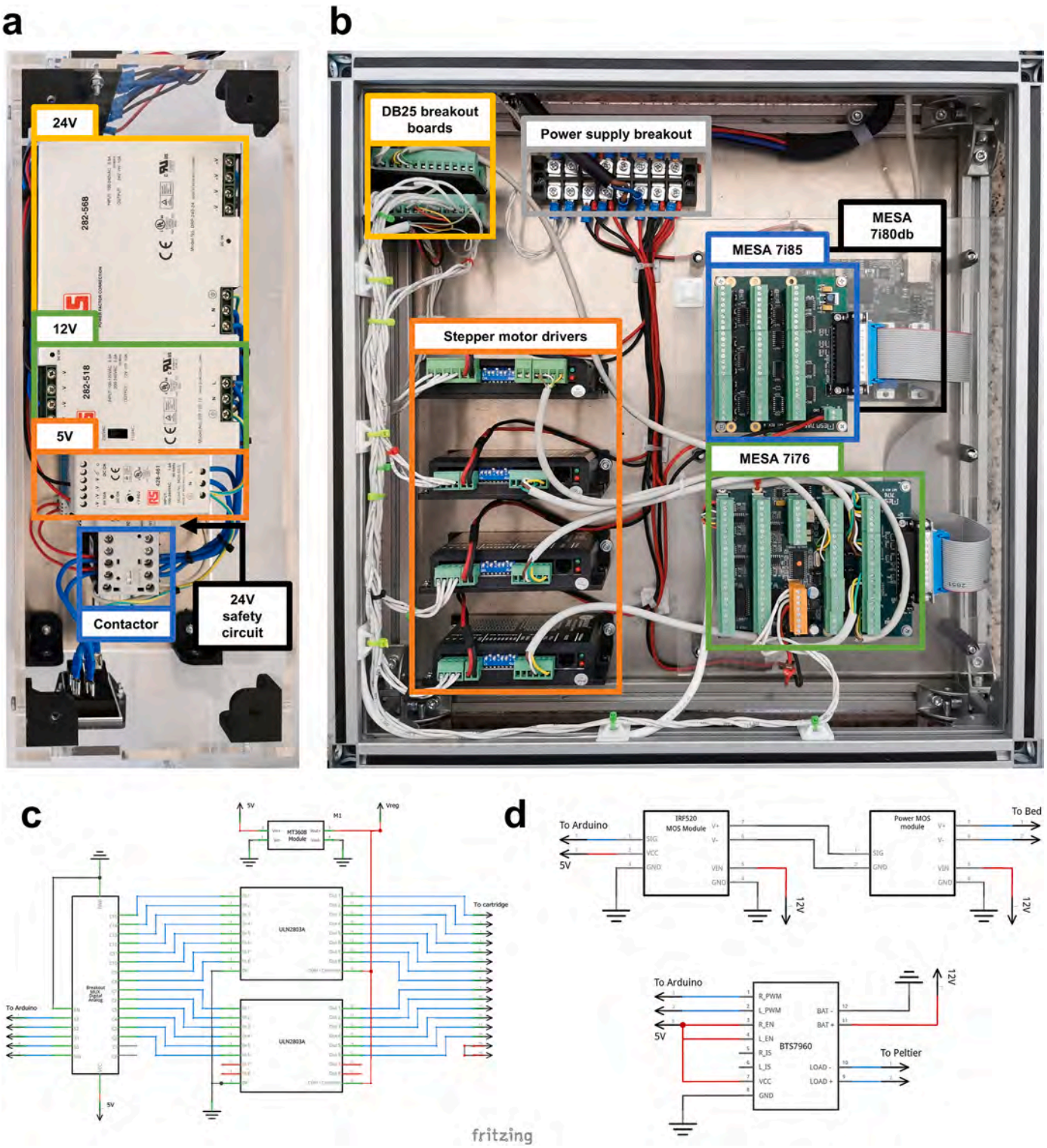


Fig. 5. Electronics module of the BOOST bioprinting platform: (a) visualization of the bioprinter power-supply modules; (b) visualization of the control module, with highlights on the different control boards and drivers; (c) a schematic of the control module for the IJB toolhead; and (d) the schematic for the additional temperature control module.

2.3.3. *Development of additional modules*

Additional hardware modules can be added to the bioprinter to extend its functionality, including for example: i) temperature control for the toolheads and the printing plate, ii) environmental control on temperature and humidity, and iii) cross-linking devices like LEDs. Among these, the BOOST bioprinter is equipped with a temperature control module consisting of a heater for the printing plate and heating/cooling system for the extruder. The former is based on a resistive heating pad (THF-90, Thermo Heating Elements), which is positioned under the printing plate. Regarding the extruder, the heating/cooling system was designed to control the temperature inside a syringe from 4 °C up to 80 °C. The system is based on a Peltier cell, a thermoelectric device which, when powered, can transfer heat from one of its sides to the other. Peltier cells represent a common solution to control the

temperature (both through heating and cooling) in many applications such as cooling devices for lasers [44]. To increase the cooling/heating efficiency of the cell, it is important to dissipate both the heat moved from one side to the other of the Peltier cell as well as the heat produced during operation of the device. As a result, the BOOST heating/cooling module features a heat dissipation system based on a commercial water cooler (Corsair H60 series) which was adapted for this specific application. In particular, the water cooler is composed of a tubing system with a pump to recirculate water. A finned heatsink equipped with a 120 × 120 mm fan is used to keep the recirculating water at room temperature, while a copper heat exchanger is placed in contact with one side of the Peltier cell. The other side of the Peltier cell exchanges heat with the syringe through a copper holder that wraps around it, as can be seen in Fig. 4.

2.4. Step 3: development of the bioprinter electronics

The electronics building block includes all the components which power and control the bioprinter. Regarding the power supply, the main parameters to be dimensioned include the operating voltage V_{supply} (measured in [V]) and the maximum current that the supply can deliver I_{supply} (measured in [A]). The choice of these parameters depends on the number and ratings of the components to be operated. For instance, the linear actuators of the BOOST positioning system operate at 24V and require 1.7 An of nominal current (Table S2). For a three axes system, this means that the power supply should be able to output at least 5.1 A. This is only a nominal value and usually a safety margin of 20 % should be considered, so that at the end a power supply operating at 24V and 6.1A is needed. A visualization of the power supply module of the BOOST bioprinter can be seen in Fig. 5a. Specifically, the printer uses three power sources: a 24V-10A power supply for the motorized axes, a 12V-10A power supply for the Peltier-based temperature control and other additional components, a 5V-10A power supply for the control boards and any other additional components. Furthermore, a contactor with a separate 24V-400 mA power supply is used for the emergency stop circuit. Key elements for the control electronics include: i) the boards that interface with the firmware, ii) the motor drivers for the positioning system, iii) the drivers for the toolheads and for any additional modules. A common solution for open source bioprinting system is to use the same control electronics of FDM printer, which usually consists in a dedicated board already including all the drivers necessary to operate the printer [45]. Although straightforward to be implemented, this solution has several limitations. Firstly, the control electronics is not tailored to a bioprinter, which means that it becomes difficult to implement other toolheads and modules different from the FDM one. Furthermore, these control electronics usually do not have high computational capacity and do not provide real-time control over the printing process, severely limiting the modularity of the developed bioprinter. In the BOOST bioprinter, the electronics is based on specialized boards (MESA Electronics) which are commonly used for the control of advanced motion systems (Fig. 5b). A field programmable gate arrays based programmable board (MESA 7i80db) is used for interfacing the bioprinter with the printer PC through an ethernet connection, while controlling two daughterboards via parallel connection, one for the motors (MESA 7i76) and the other for the encoders (MESA 7i85). Four stepper drivers (DM442, Leadshine) are used to actuate each printer axis (X, Y, and Z for the positioning, and A for the extrusion of FDM and EBB toolheads). The control module is connected to the printer through two DB25 breakout boards, which handle all low-amperage signals, while the power cables from the power supply are distributed i) inside the control thanks to a high-amperage breakout board, and ii) directly to the printing module through plug-and-play connectors.

Moreover, custom control boards were designed and implemented for the IJB toolhead and the temperature control module, as can be seen in Fig. 5c and in Fig. 5d respectively. To print a dot of ink, the cartridge needs to receive a specific signal from the control board with a voltage that depends on the solution properties (i.e., viscosity, and surface tension). The inkjet cartridge is controlled by an Arduino Nano which, depending on the input from the printer PC sent through serial communication, excites each nozzle separately with a user-defined voltage. To decrease the number of needed pins on the Arduino board, a solution based on a demultiplexer (CD74HC4067, Texas Instruments) was designed. In particular, the demultiplexer has 4 inputs (from the Arduino board) and 16 outputs. 12 of these outputs are sent to two separate Darlington arrays (ULN2803A, Texas Instruments), which are used to reach an appropriate signal load to excite a nozzle with a separate boost converter (MT3608, AZDelivery). The latter takes as input 5V directly from the power supply module of the printer and increases it thanks to an internal potentiometer. The user can manually modify this output voltage by rotating the knob of the potentiometer and viewing the current value via an LCD screen placed on the inkjet control box lid.

Regarding the extruder heating/cooling system, an H-bridge (BTS7960, Lrtzizy) was used since it can switch the polarity of the output voltage enabling both cooling and heating with the same Peltier element (Fig. 5d). The temperature of the copper syringe holder is monitored through a commercial temperature probe (DS18B20, AZDelivery), with the wires isolated from the outside using a rubber sheath to prevent faulty readings due to condensation water during operation. An Arduino Uno board is used to read the temperature and control the output current from the H-bridge by a pulse width modulation (PWM) signal. The H-bridge used for the Peltier cell in the extruder can also be employed for the FDM tool head, by switching between the two using plug-and-play connectors. Finally, a similar system based on a MOSFET (NCEP01T18T, 'bed MOS' in Fig. 5d) is used to control the temperature of the printing bed (measured through an NTC thermistor), as can be seen in the schematics of Fig. 5d.

2.5. Step 4: development of the bioprinter software

Since commonly used electronics for bioprinters are based on FDM control boards, the firmware and software toolchain to operate those printers is the same as the one for FDM. In the typical FDM workflow, a g-code file (i.e., a text file containing all the necessary machine instructions to produce the printed object) is read by a specialized firmware, a piece of software able to interpret the g-code instructions and translate them into a physical operation by the printer. Commonly used firmware distributions in FDM include Marlin, RepRap firmware, and Klipper. Even though customization to the latter have already been successfully reported [24,37], to the best of our knowledge there is no firmware specifically tailored to bioprinting. Ideally, this firmware should be able to operate multiple and diverse bioprinting technologies, ranging from the extrusion processes of EBB and FDM up to the material jetting ones of IJB. Furthermore, the firmware should be compatible with already existing software tools for AM to generate the g-code to be easily adopted by researchers. Herein, we propose LinuxCNC as an effective firmware that meets these requirements and that can thus be customized effectively to develop advanced multimaterial and multiscale bioprinters.

2.5.1. Overview of the software architecture

The BOOST bioprinter is controlled through LinuxCNC, a software for numerical control of machines, such as milling machines, lathes, cutting machines, robots [46,47]. It can control up to 9 axes of a CNC machine using g-code as input. The main attributes of LinuxCNC are its modularity and flexibility, allowing easy integration of different new components into an already existing system. These properties are a consequence of its software architecture, which is composed of five main layers: i) a graphical user interface (GUI); ii) the task executor (EMC-TASK), as command handler and program interpreter for the g-code; iii)

Table 3
summary of the configurations set for the three axes of the positioning system.

Parameter name		Value	Unit of measure
X axis	MIN_LIMIT/MAX_LIMIT	−0.01/200	[mm]
	STEP_SCALE	−3200	[steps/mm]
	DIRSETUP/DIRHOLD/STEPLEN/STEPSPACE	5000/5000/5000/5000	[ns]
	MAX_VELOCITY	20	[mm/s]
	MAX_ACCELERATION	250	[mm/s^2]
	HOME	5	[mm]
Y axis	MIN_LIMIT/MAX_LIMIT	−0.01/150	[mm]
	STEP_SCALE	−3200	[steps/mm]
	DIRSETUP/DIRHOLD/STEPLEN/STEPSPACE	5000/5000/5000/5000	[ns]
	MAX_VELOCITY	20	[mm/s]
	MAX_ACCELERATION	250	[mm/s^2]
	HOME	5	[mm]
Z axis	MIN_LIMIT/MAX_LIMIT	−0.01/150	[mm]
	STEP_SCALE	−3200	[steps/mm]
	DIRSETUP/DIRHOLD/STEPLEN/STEPSPACE	5000/5000/5000/5000	[ns]
	MAX_VELOCITY	20	[mm/s]
	MAX_ACCELERATION	250	[mm/s^2]
	HOME	5	[mm]

the motion controller (EMCMOT), that performs trajectory planning and direct and inverse kinematics, driving the motor control subsystems; iv) the I/O controller (EMCIO), a single input/output controller which handles all functions that are not related to motion control; v) the hardware abstraction layer (HAL), the lowest level of the software architecture, a system that masks what is behind each hardware component with simple black box-like software components.

The configuration for the bioprinter is based on a standard configuration file for a three axes cartesian machine. The associated configuration file (in.ini format) was modified with the appropriate parameters for the chosen positioning system, including.

- Travel range (MIN_LIMIT, MAX_LIMIT), which is set according to the linear stage specifications of Table 3;
- Steps/mm (STEP_SCALE), which defines for each axis how many steps of the stepper motor are required to obtain a movement of 1 mm. This parameter depends on i) the transmission type and ratio used by the axis, ii) the stepper motor characteristics, and iii) the use of micro-stepping in the motor driver. For example, considering the case of the linear stages in Table 3, the stepper motor uses 200 full steps to complete a revolution, and each full step is composed of 64 micro-steps, for a total of 200x64 = 12800 micro-steps per revolution. The stepper motor is directly attached to a leadscrew system so that a full revolution of the motor axis corresponds to a linear displacement equal to the leadscrew pitch, which for the chosen system is 1 mm. The final parameter is then equal to 12800 steps/mm;
- Temporization of the pulse signal (DIRSETUP, DIRHOLD, STEPLEN, STEPSPACE), which depends on the stepper motor driver and is reported on the related datasheet;
- Maximum speed and acceleration for each axis (MAX_VELOCITY, MAX_ACCELERATION), chosen according to the linear stage specifications;
- Home position (HOME), which depends on the position of the limit switches mounted on the linear stages, and homing sequence, which determines the order of the homing procedure.

A summary of the main modifications done in the machine configuration file can be found in Table 3.

Once the basic configuration for the bioprinter was defined, software modifications were performed to control the toolheads and the additional modules. Regarding the extruder control, the extruder stepper motor was configured in LinuxCNC as axis A, and its parameters were set with the same logic as the other linear stages. The steps/mm value was set using the transmission ratios of the composite mechanism (as can be seen in Table S3). Similar modifications were made for the FDM toolhead, where the steps/mm value was set according to the transmission ratio reported in the extruder datasheet.

Custom toolheads and modules can be controlled through the pipeline defined in Fig. 6, which defines a method to send a command from LinuxCNC to a connected Arduino board through serial communication. Specifically, a user defined M command (in the range M100-M199 as specified by the LinuxCNC documentation), is firstly created as a bash script. Parameters can be passed alongside the M code using a 'P' value. When the LinuxCNC EMCTASK reads the command, the program defined in the M code is triggered and a variable (a 'pin' in the HAL nomenclature) inside a custom-defined HAL component is set to the value passed in the 'P' variable of the M code. A custom Python program (v2.7, version compatible with the LinuxCNC distribution) is then used to encode this variable and send it through serial communication to the connected Arduino board. In the latter, a firmware waits for the message, decodes it, and performs the related task. Both the inkjet toolhead

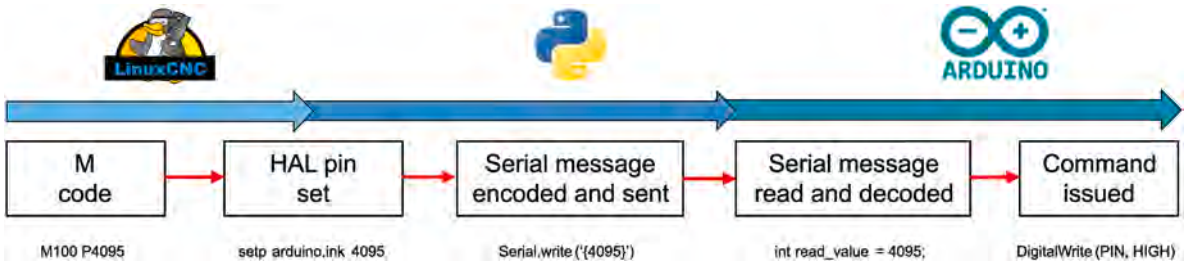


Fig. 6. Summary of the pipeline to send a command from LinuxCNC to an Arduino board connected to the PC through serial communication showing an example of user defined M command to control the inkjet toolhead in the BOOST bioprinter (i.e., M100 P4095).

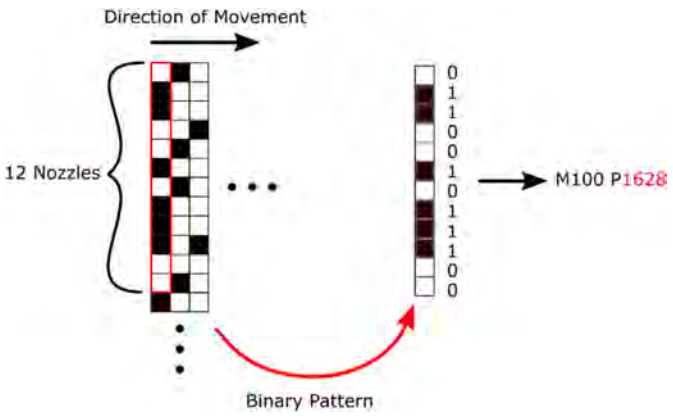


Fig. 7. Example conversion of a binary image to ink g-code, in red the selected pattern (twelve rows and one column). (For interpretation of the references to colour in this figure legend, the reader is referred to the Web version of this article.)

and the temperature module are controlled using this logic. Briefly, an integer value between 1 and 4095 is sent to the Arduino board based on a user defined M command (e.g., M100 PX, where X represents the integer to be sent) which triggers the printing of a line. The pattern codifies which of the twelve nozzles must be active at any given time to print. On the Arduino board, after receiving the value through serial, the firmware performs a conversion of the integer to a 16-bit binary representation. The first four bits are not enabled, while the other twelve directly command the twelve corresponding nozzles (i.e., a bit equal to 1 means that the nozzle should print, while it should not print if equal to 0). Based on the electronics implementation, the four pins commanding the multiplexer are then set to the correct value and the printing is performed. A similar approach was also employed to control temperature additional module. The module is controlled through three separate user defined M commands (M140 for the bed temperature control, M141 for the FDM toolhead, and M102 for the heating/cooling system), in which the P parameter specifies the set temperature. Based on the sent value, the Arduino board issues a PWM signal to the MOSFET/H-bridge depending on the M command to reach the targeted temperature. Internally, the PWM signal is regulated by a PID controller.

2.5.2. *Pipeline to print with two toolheads in the same process*

Thanks to the previously described tool-changer system, the bioprinter can use two different toolheads at the same time from the following combinations: i) fixed syringe extruder and inkjet mounted on the tool-changer; ii) fixed FDM and inkjet mounted on the tool-changer. Each toolhead can be used either separately or together with the other mounted one by using an ad-hoc defined g-code file. The following paragraphs will detail the necessary steps to produce the g-code file for each tool head and their combination.

2.5.2.1. Extrusion and FDM g-code generation. The extrusion and FDM g-code files are handled in the same way since the working principle is similar for both. In particular, the g-code is produced by a standard STL slicer (e.g., Slic3r, Cura, etc.). Specific printing settings depending on the toolhead to be used should be decided at this stage. Particular attention should be taken to set the 'nozzle diameter' and 'filament diameter' parameters for the extrusion toolhead. In this case, the 'nozzle diameter' parameter should be set to the internal diameter of the chosen syringe needle. Since common slicers use conservation of mass equations to compute the amount of material to be extruded for a given line length [48], to obtain correct extrusion rates the 'filament diameter' parameter should be set to the internal diameter of the syringe (i.e., equal to 12 mm for standard 5 ml syringes). The output g-code file from the slicer may have some commands that cannot be interpreted, or that have different results than intended when read by LinuxCNC. As a result, the file is filtered through a custom post-processing Python script that converts all the 'E' of the extrusion (the standard name for the extrusion axis in other firmware) with 'A' (the name of the extrusion axis in LinuxCNC), removes all the comments and the M commands. The output of the filtering procedure can be directly printed as is or can be merged with the inkjet g-code following the procedure described in the following sections.

2.5.2.2. Inkjet g-code generation. The inkjet g-code generation procedure starts with a single, binary image, representing the pattern to be printed. The image is read by a custom Python program as a matrix of '0s' (black) and '1s' (white) where each black cell corresponds to an ink drop ejected through a single nozzle. The image matrix is then scanned from left to right (Fig. 7). For each column, the algorithm takes twelve rows, corresponding to the twelve nozzles of the cartridge, reads the corresponding binary number, and converts it to an integer. The M100 code is written in the output g-code file, with the P parameter set to the converted value. Each print move is then followed by a movement command G1 (i.e., a linear movement with a specified feed-rate). During a single partial scan (twelve rows, all the columns), the Y coordinate is constant, while the X one is incremented by the horizontal resolution specified by the user.

Once all the columns have been scanned, the algorithm reads the columns of the following twelve rows and so on, until the whole matrix has been scanned. After each partial scan, the Y coordinate is incremented of a fixed value, equal to the number of nozzles times the spacing of the nozzles ($12 \times 0.26 = 3.12\,mm$), until the whole image has been scanned.

2.5.2.3. Merged g-code generation. The two separate g-code files, one for the mechanical extruder/FDM module and one for inkjet, can be merged by defining a custom procedure to switch between the two techniques. In particular, a custom M-code command (M101 PX, where X defines the type of movement) was implemented in LinuxCNC to control the tool-changer movement. The command uses a parameter P which can be either 1 or 2; if P is equal to 1 the tool-changer is moved upwards by a specified servo motor rotation and the inkjet module will not print. On the other hand, if P is equal to 2, the tool-changer is moved downwards until it reaches the mechanical stop. In this configuration, the tool attached to the tool-changer is used for printing. When moving from an extrusion printing path to the inkjet module, the following procedure is coded into the g-code.

1. Move the Z-axis of the machine up to avoid the collision of the cartridge with the printing support;
2. Move the printing plate so that the cartridge is positioned at its center. At this point, the cartridge is well above the printing plate, so a M101 P2 command is issued to move it at $\approx$ 5 mm above the printing surface;
3. A G4 command follows all the cartridge movements, which issues a dwell move (the printer does nothing) for a number of seconds specified by its P value; during this interval, the interpreter stops reading and executing the successive lines.

After printing with inkjet, the transition to extrusion follows the same logic, but with a mirrored procedure.

1. The cartridge is moved down with an M101 P1 command, immediately followed by a dwell move G4;
2. The building plate is moved backwards, so that the tip of the syringe is at the centre of the print;
3. The Z-axis is moved down to reposition the tip at the proper height.

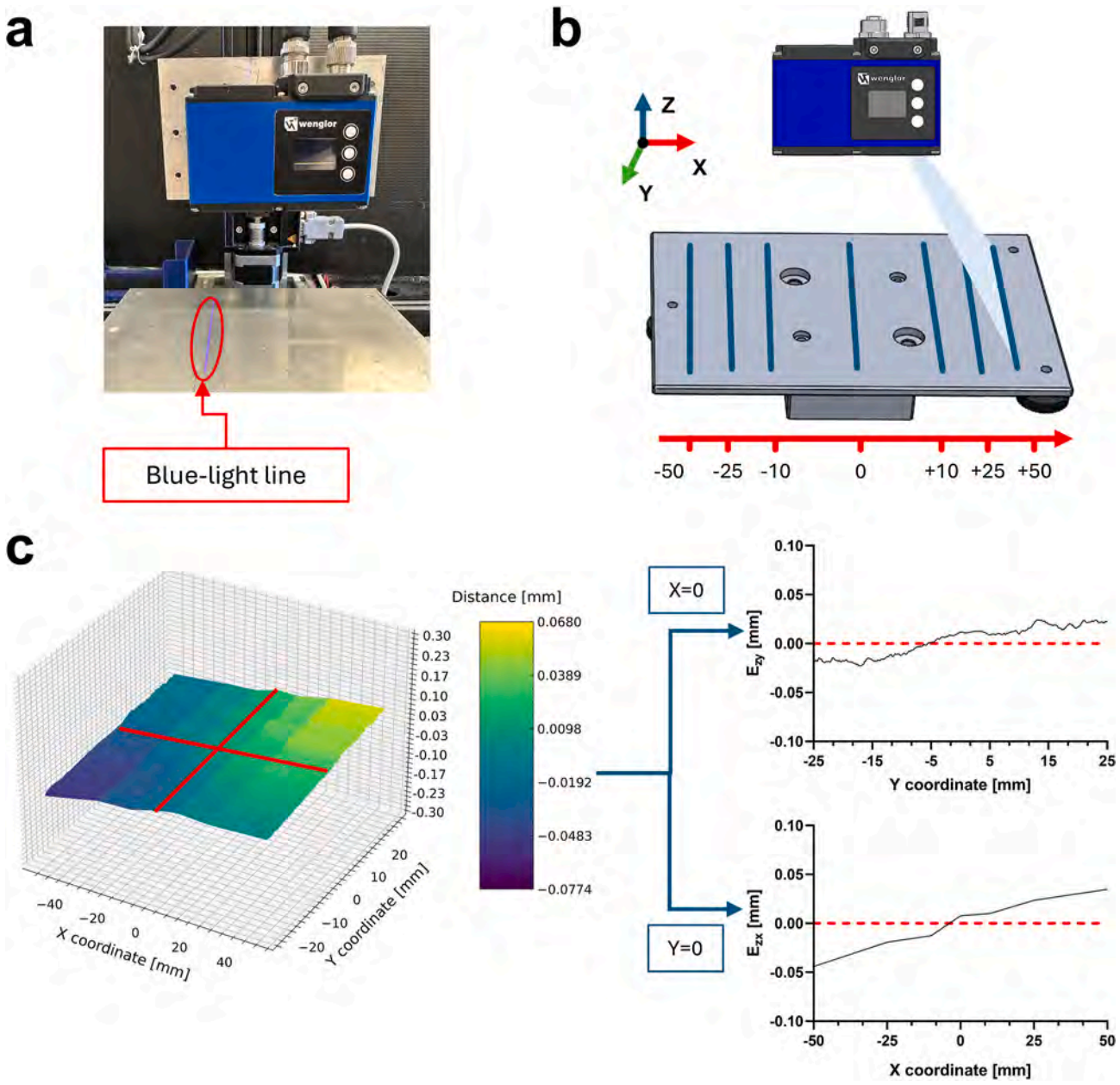


Fig. 8. Summary of the experiments to validate the straightness of the positioning system. In (a), a photo of the set-up, showing the blue-light distance sensor mounted on the toolhead plate. In (b), overview of the scanning procedure, in which the distance is acquired at different X positions. Finally, in (c) the results for the straightness analysis in the Z-X and Z-Y planes. (For interpretation of the references to colour in this figure legend, the reader is referred to the Web version of this article.)

3. Platform validation

Extensive examples on using the platform with single technologies has been already reported elsewhere, like for instance the creation of an extensive dataset of videos recording the extrusion-printing process for Machine Learning models training and testing [49,50], or the validation of mathematical models of the EBB process [48]. Herein, we validate the previously presented design workflow by: i) measuring the quality of the positioning system and the accuracy and repeatability of the printing process, and ii) demonstrating the capability of the bioprinter to produce multimaterial and multiscale scaffolds by combining different techniques together in a single fabrication process.

3.1. Measuring accuracy and repeatability of the BOOST bioprinter

We conducted two set of experiments to quantitatively evaluate the ability of the BOOST bioprinter to produce high quality, repeatable scaffolds for TE applications. In the first set, a blue-light profile sensor (MLSL132 2D/3D, Wenglor, with a resolution of 30 μm for distance measurements) was mounted on the toolhead plate through a custom-made 3D printed support, with the blue-light line of the sensor parallel to the Y axis of the printer (Fig. 8a). Distance data from the sensor were acquired to investigate the straightness error (i.e., unwanted motion in one of the two directions orthogonal to the direction of a linear axis commanded to move along a (nominal) straight-line trajectory, as defined in the standard ISO-230–1:2012, Part 1: Geometric accuracy of machines operating under no-load or quasi-static conditions) in the Z-X (E_{zx}) and Z-Y (E_{zy}) planes when issuing a movement along the X and Y

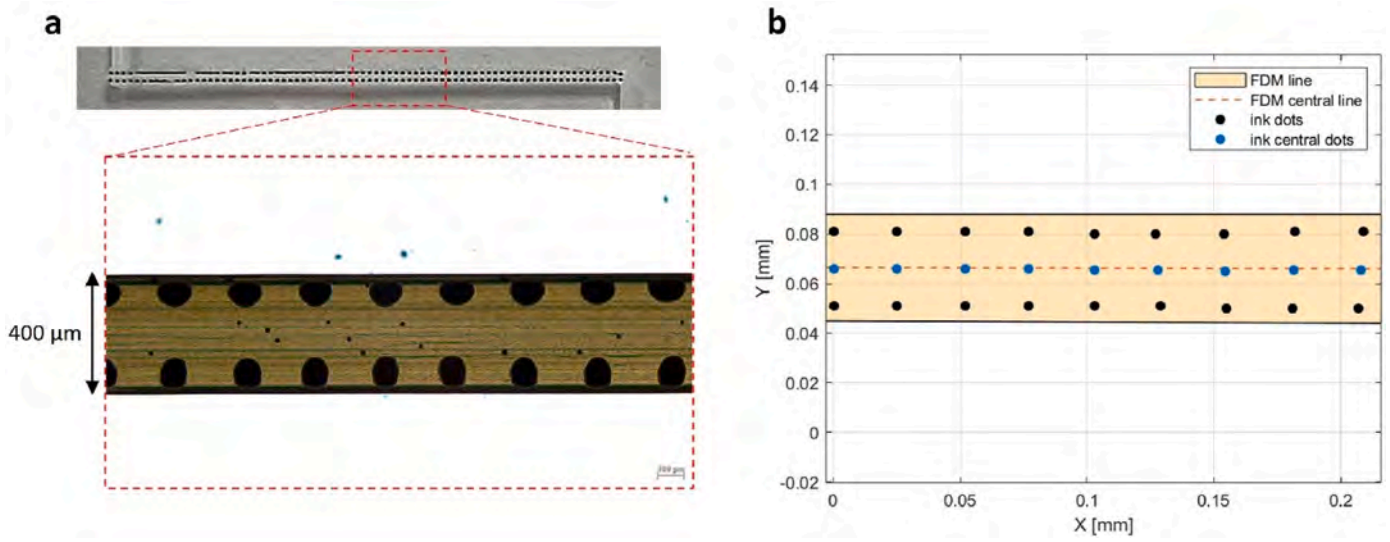


Fig. 9. Single-step combination – Printheads calibration: (a) Calibration test of the two printheads by depositing black ink on a FDM printed line; (b) Estimation of the calibration error as the distance between the central FDM line and the central ink dots.

coordinates, respectively. Specifically, after homing the printer the bed was moved in increments along the X axis (i.e., −50 mm, −25 mm, −10 mm, 0, +10 mm, +25 mm, +50 mm, where the 0 position refers to the bed center along the X axis). For each increment, the whole distance line (spanning from around −25 mm to + 25 mm, where the 0 position refers to the bed center along the Y axis) was used to acquire the distance along the Z axis parallel to the Y axis (Fig. 8b). All measurements were done at room temperature and the acquisition was performed waiting at least 3 s after the movement end to have a stable acquisition. The data acquired was then filtered to smooth the sensor response (moving average filter, using a window of 30 samples) and plotted, as reported in Fig. 8c. As can be seen from the figure, the straightness error in the two planes shows comparable values, with the maximum value for E_{zx} at around 35 µm and for E_{zy} at around 28 µm. These values are of the same order of magnitude of the distance sensor resolution, and, together with the high accuracy and repeatability of the single axis, highlight the high quality of the positioning system.

In the second set of experiments, a total of 50 scaffolds (i.e., cylinder shape of 5 mm diameter and 1 mm height, 1 perimeter and 50 % infill density, no bottom or top layers) were printed using the FDM module with commercial PLA (Filoprint) as model material to test the repeatability of the printing process. The scaffold dimensions and shape were chosen according to a previous work by our group, focusing on the printing of scaffolds for bone tissue engineering [13]. After printing,

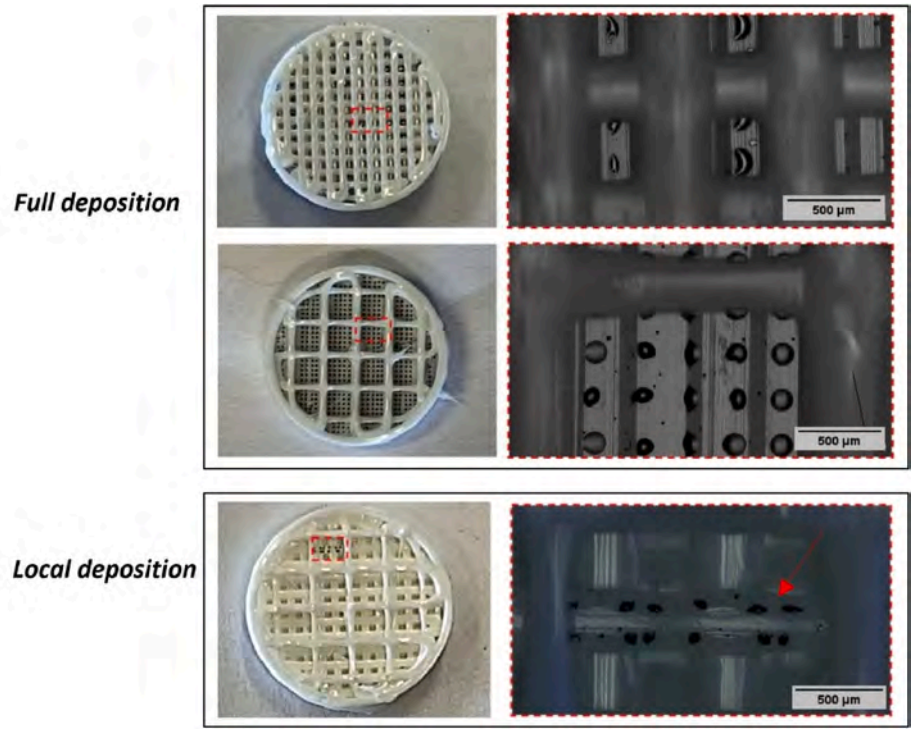


Fig. 10. Single-step combination: 3D printed white PLA scaffolds with fully/locally (pointed with a red arrow) deposited black ink within the scaffold architecture. (For interpretation of the references to colour in this figure legend, the reader is referred to the Web version of this article.)

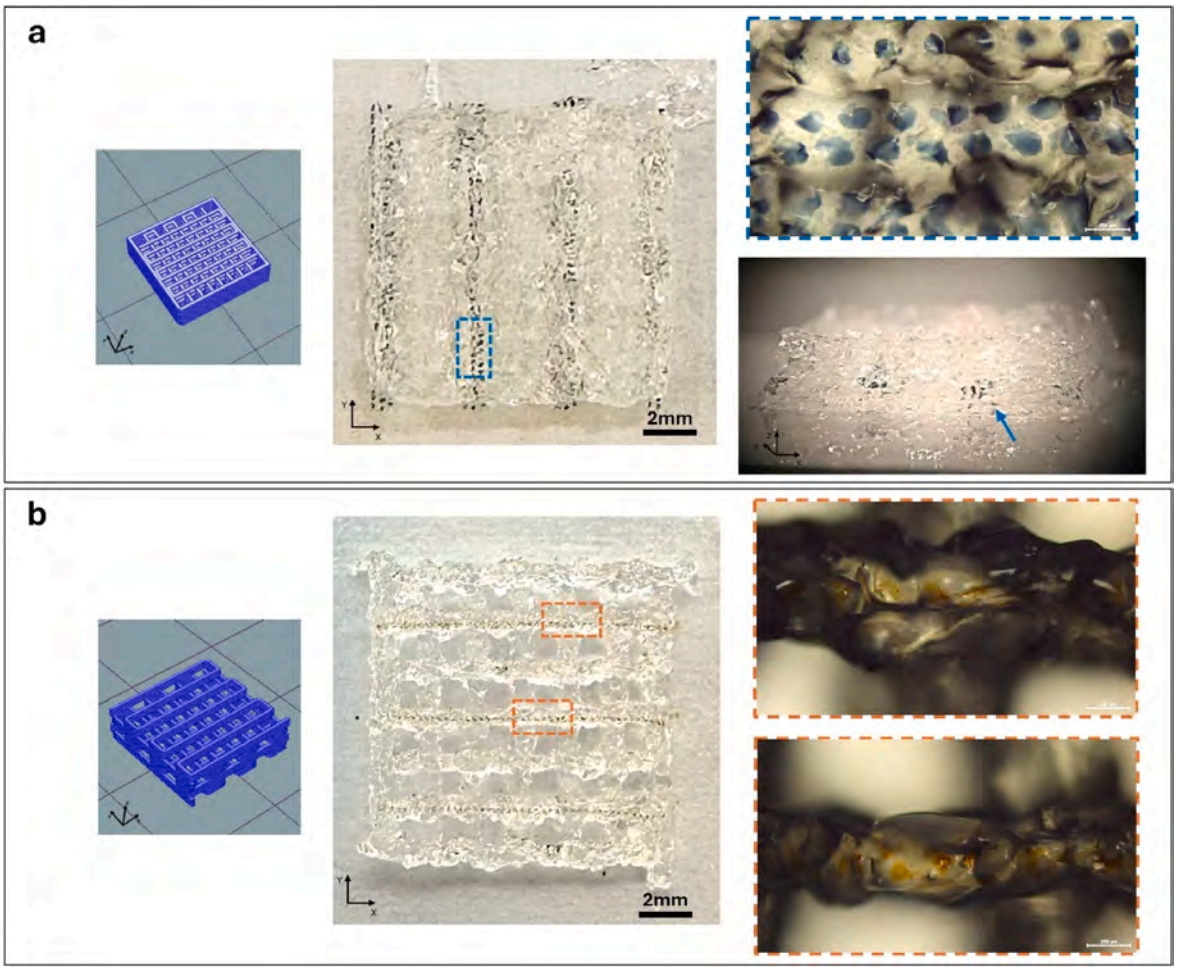


Fig. 11. EBB and IJB combination to create multiscale and stimuli-responsive scaffolds. In (a), IJB of a solution of PEDOT:PSS to create electric conductive tracks within the scaffold, and in (b) of an aqueous dispersion of magnetic nanoparticles (i.e., SPIONs) on the strands of a woodpile scaffold that can be used to directly stimulate cells by the application of a magnetic field.

each scaffold was measured using a digital caliper to measure its diameter and height. The results are reported in Figure S1 of the Supplementary Materials. As can be seen from the figure, the measurements are close to the targeted ones for both dimensions, reaching a mean value of 4.97 mm for the diameter and of 1 for the height. The accuracy of the printed scaffolds (computed as the standard deviation of the difference between the measurement and the designed value for the diameter/height) was measured as 56 and 27 μm, which is below that of commercial FDM printers (±100 μm [51]).

3.2. *Multimaterial and multiscale bioprinting with the BOOST bioprinter*

To show the capability of the bioprinter to produce multimaterial and multiscale constructs, we firstly devised a procedure using the combination of FDM and IJB. The choice of these two technologies as the starting point was done to have constructs that could be easily imaged to see the local functionalization of polymeric materials with ink droplets. Specifically, commercial white PLA (Filoprint) was used as a model material for FDM, while black ink as the model material for the IJB process. Firstly, a calibration procedure was performed to align the two toolheads. During calibration, a 20 mm-long line was FDM printed with the PLA filament, and then black ink was deposited on the line by activating the two central nozzles of the cartridge. The line was examined under an optical microscope (LEICA DM6 M, using top illumination at 100× magnification) to calculate the absolute error between the central FDM-printed line and the ink dots (Fig. 9a). Images were analysed in ImageJ [52] to estimate the coordinates of the FDM-printed line and the centres of the ink dots (Fig. 8b). Data were then loaded in MATLAB (R2022b) software to compute the calibration error. For each couple of ink dots, the midpoint coordinates were computed (namely, ink central dots). Similarly, the midline of the FDM-printed line was calculated (namely, FDM central line). The calibration error was estimated as the absolute difference between the coordinates of the FDM-printed central line and that of the ink central dots. An error of 5 ± 2 μm was obtained after calibration, which is in accordance with the nominal resolution of the linear stages (i.e., 5 μm). Once the two toolheads were properly calibrated, the single-step combination was performed by alternating between FDM printing of standard white PLA layers and the full/local inkjet deposition of black ink to fabricate multimaterial and multiscale cylindrical scaffolds (10 mm diameter and 1.8 mm height) (Fig. 10). Three different printing patterns are shown in Fig. 10. In the first and second cases, the scaffold consists of a bottom 3D printed layer (i.e., 0 % porosity), black ink fully deposited on the area, and a final 50 % or 20 % porosity 3D printed layer. In the third case, the scaffold has a bottom layer, an intermediate layer of 50 % porosity and a line of black ink locally deposited on a strand, and a final 3D printed layer of 10 % porosity.

Based on the previously validated procedure, the printing of scaffolds using biomaterials was demonstrated by combining EBB with IJB, showing the ability of the BOOST bioprinter to create multimaterial and multiscale scaffolds. For EBB, a biomaterial ink was obtained by mixing pectin and gelatin (named Gel-Pect) as previously described [53,54],

printed with a speed of 3 mm/s, a layer height of 0.3 mm and using a 21G needle. For IJB two different solutions where used, namely, an organic conductive polymer solution of PEDOT:PSS, and a water dispersion of magnetic nanoparticles of SPIONs, with the aim to create scaffolds that can react to external stimuli, electric and magnetic, and thus trigger a specific biological behaviour. In the first case, a cubic scaffold of 10x10 × 5mm was printed by alternating the extrusion of the Gel-Pect hydrogel and the local deposition of PEDOT:PSS to create a pattern of localized conductive tracks. Droplets were successfully incorporated into the hydrogel layers as shown in Fig. 11a. Once seeded with cells, the conductive tracks can potentially provide them electrical stimuli, for instance, to guide and enhance the muscle regeneration [55]. In the second example, the SPIONs-loaded solution was locally jetted on the strands of a woodpile structure (10x10 × 3 mm, 1.2 mm pores, 0.6 mm strands), which were successfully and precisely deposited as illustrated in Fig. 11b. In this way, cells can be directly exposed to SPIONs once seeded onto the scaffolds to trigger, for instance, their mechano-transduction in presence of a magnetic field in the bone tissue engineering [56]. Dimensions of the pores and strands of the printed scaffold were measured using ImageJ software, resulting 1.06 ± 0.11 mm and 0.74 ± 0.06 mm, respectively, resulting in a relative error of 28 % and 24 %. Although less accurate than the measurements for FDM, these errors might depend on the material rheological properties that might induce an uneven extrusion.

4. Conclusions

Bioprinting represents a promising technology for the fabrication of scaffolds for TE applications. In recent years, a major trend in bioprinting research is represented by the combination of multiple AM techniques, each operating at different scale lengths and each being compatible with different materials, to create complex structures that more closely mimic the natural composition of the targeted tissue extracellular matrix. Although several companies have started commercializing bioprinters, open source projects are also available in literature, which usually employ modifications of already existing printers and adapt them to the specifics of bioprinting. In this context, here we described a design workflow to fabricate a bioprinter from the ground up, taking into consideration all the necessary requirements and constraints. The proposed workflow starts with the definition of the design requirements that should be considered during the initial stage of the process, including for instance the number and type of bioprinting technologies that should be used, or the overall weight and encumbrance of the final platform. Using these requirements, the workflow proposes robust methods to design the main components of a bioprinting system, namely the hardware (i.e., the positioning system, toolheads, and additional modules), electronics (i.e., power supply, control boards), and software (i.e., firmware, methods to generate the g-code). Following this workflow, we described the development of the BOOST bioprinter, an open source multimaterial and multiscale bioprinter (compatible with three technologies, namely EBB, FDM, and IJB) able to produce high quality scaffolds. The firmware source code is made available online in the ZENODO repository (https://doi.org/10.5281/zenodo.10993098) and will serve as a blueprint for the development of advanced, open source bioprinters.

CRediT authorship contribution statement

Amedeo Franco Bonatti: Writing – original draft, Validation, Software, Methodology, Investigation, Formal analysis. **Elisa Batoni:** Writing – original draft, Validation, Software, Methodology, Investigation, Formal analysis. **Gabriele Maria Fortunato:** Writing – review & editing, Methodology, Formal analysis. **Chiara Vitale-Brovarone:** Supervision, Funding acquisition. **Giovanni Vozzi:** Supervision, Funding acquisition. **Carmelo De Maria:** Writing – review & editing, Methodology, Funding acquisition, Conceptualization.

Declaration of competing interest

The authors declare that they have no known competing financial interests or personal relationships that could have appeared to influence the work reported in this paper.

Acknowledgments

This project has received funding from the European Research Council (ERC) under the European Union's Horizon 2020 research and innovation program (grant agreement No. 681798-BOOST) (www.ercprojectboost.eu). This study received funding from the European Union - Next-GenerationEU - National Recovery and Resilience Plan (NRRP) – Mission 4 Component 2, investment n. 1.1, Prin 2022 – Prometheus "4D printing self-deploying bio-enabled polymer scaffolds for the non-invasive treatment of bleeding intestinal ulcers", grant: 2022BZLTTK, CUP I53D23002200006. The work has been partially supported by the Italian Ministry of University and Research (MUR) in the framework of the FoReLab project (Departments of Excellence). We also acknowledge the support of the European Union by the Next Generation EU project ECS00000017 'Ecosistema dell'Innovazione' Tuscany Health Ecosystem (THE, PNRR, Spoke 4: Nanotechnologies for diagnosis and therapy), and of the Crosslab Additive Manufacturing of the Department of Information Engineering of the University of Pisa.

Appendix A. Supplementary data

Supplementary data to this article can be found online at https://doi.org/10.1016/j.bprint.2024.e00372.

Data availability

Data will be made available on request.

References

[1] L. Moroni, T. Boland, J.A. Burdick, C. De Maria, B. Derby, G. Forgacs, G. Vozzi, Biofabrication: a guide to technology and terminology, Trends Biotechnol. 36 (4) (2018) 384–402, https://doi.org/10.1016/j.tibtech.2017.10.015.
[2] J. Groll, J.A. Burdick, D.W. Cho, B. Derby, M. Gelinsky, S.C. Heilshorn, T.B. F. Woodfield, A definition of bioinks and their distinction from biomaterial inks, Biofabrication 11 (1) (2018) 013001, https://doi.org/10.1088/1758-5090/aaec52.
[3] A.F. Bonatti, G.M. Fortunato, C. De Maria, G. Vozzi, Bioprinting technologies: an overview, in: M. Conti, M. Marino (Eds.), Bioprinting: from Multidisciplinary Design to Emerging Opportunities, Academic Press, 2022, pp. 19–49.
[4] S. Santoni, S.G. Gugliandolo, M. Sponchioni, D. Moscatelli, B.M. Colosimo, 3D bioprinting: current status and trends—a guide to the literature and industrial practice, Bio-Design and Manufacturing 5 (1) (2022) 14–42, https://doi.org/10.1007/s42242-021-00165-0.
[5] I.T. Ozbolat, M. Hospodiuk, Current advances and future perspectives in extrusion-based bioprinting, Biomaterials 76 (2016) 321–343, https://doi.org/10.1016/j.biomaterials.2015.10.076.
[6] F. Pati, J. Jang, J.W. Lee, D.W. Cho, Extrusion bioprinting, in: A. Atala, J. Yoo (Eds.), Essentials of 3D Biofabrication and Translation, Academic Press, 2015, pp. 123–152.
[7] A. Leucht, A.C. Volz, J. Rogal, K. Borchers, P.J. Kluger, Advanced gelatin-based vascularization bioinks for extrusion-based bioprinting of vascularized bone equivalents, Sci. Rep. 10 (1) (2020) 5330, https://doi.org/10.1038/s41598-020-62166-w.
[8] I. Chiesa, C. De Maria, A. Lapomarda, G.M. Fortunato, F. Montemurro, R. Di Gesù, R. Gottardi, Endothelial cells support osteogenesis in an in vitro vascularized bone model developed by 3D bioprinting, Biofabrication 12 (2) (2020) 025013, https://doi.org/10.1088/1758-5090/ab6a1d.
[9] K. Flégeau, A. Puiggali-Jou, M. Zenobi-Wong, Cartilage tissue engineering by extrusion bioprinting utilizing porous hyaluronic acid microgel bioinks, Biofabrication 14 (3) (2022) 034105, https://doi.org/10.1088/1758-5090/ac6b58.
[10] A. Sadeghianmaryan, S. Naghieh, H.A. Sardroud, Z. Yazdanpanah, Y.A. Soltani, J. Sernaglia, X. Chen, Extrusion-based printing of chitosan scaffolds and their in vitro characterization for cartilage tissue engineering, Int. J. Biol. Macromol. 164 (2020) 3179–3192, https://doi.org/10.1016/j.ijbiomac.2020.08.180.
[11] H. Liu, K. Gong, A. Portela, Z. Cao, R. Dunbar, Y. Chen, Granule-based material extrusion is comparable to filament-based material extrusion in terms of mechanical performances of printed PLA parts: a comprehensive investigation, Addit. Manuf. 75 (2023) 103744, https://doi.org/10.1016/j.addma.2023.103744.

[12] A.R. Calore, R. Sinha, J. Harings, K.V. Bernaerts, C. Mota, L. Moroni, Additive Manufacturing Using Melt Extruded Thermoplastics for Tissue Engineering, Springer US, 2021, pp. 75–99, https://doi.org/10.1007/978-1-0716-0611-7_7.

[13] G.I. Kontogianni, A.F. Bonatti, C. De Maria, R. Naseem, P. Melo, C. Coelho, M. Chatzinikolaidou, Promotion of in vitro osteogenic activity by melt extrusion-based PLLA/PCL/PHBV scaffolds enriched with nano-hydroxyapatite and strontium substituted nano-hydroxyapatite, Polymers 15 (4) (2023) 1052, https://doi.org/10.3390/polym15041052.

[14] A. Grémare, V. Guduric, R. Bareille, V. Heroguez, S. Latour, N. L'heureux, D. Le Nihouannen, Characterization of printed PLA scaffolds for bone tissue engineering, J. Biomed. Mater. Res. 106 (4) (2018) 887–894, https://doi.org/10.1002/jbm.a.36289.

[15] W. Wang, B. Zhang, M. Li, J. Li, C. Zhang, Y. Han, X. Zhang, 3D printing of PLA/n-HA composite scaffolds with customized mechanical properties and biological functions for bone tissue engineering, Compos. B Eng. 224 (2021) 109192, https://doi.org/10.1016/j.compositesb.2021.109192.

[16] M. Yanez, J. Rincon, A. Dones, C. De Maria, R. Gonzales, T. Boland, In vivo assessment of printed microvasculature in a bilayer skin graft to treat full-thickness wounds, Tissue Eng. 21 (1–2) (2015) 224–233, https://doi.org/10.1089/ten.tea.2013.0561.

[17] S. Hewes, A.D. Wong, P.C. Searson, Bioprinting microvessels using an inkjet printer, Bioprinting 7 (2017) 14–18, https://doi.org/10.1016/j.bprint.2017.05.002.

[18] X. Li, B. Liu, B. Pei, J. Chen, D. Zhou, J. Peng, T. Xu, Inkjet bioprinting of biomaterials, Chem. Rev. 120 (19) (2020) 10793–10833, https://doi.org/10.1021/acs.chemrev.0c00008.

[19] B. Derby, Inkjet printing of functional and structural materials: fluid property requirements, feature stability, and resolution, Annu. Rev. Mater. Res. 40 (2010) 395–414, https://doi.org/10.1146/annurev-matsci-070909-104502.

[20] D. Choudhury, S. Anand, M.W. Naing, The arrival of commercial bioprinters–Towards 3D bioprinting revolution, International Journal of Bioprinting 4 (2) (2018), https://doi.org/10.18063/IJB.v4i2.139.

[21] J.W. Tashman, D.J. Shiwarski, A.W. Feinberg, Development of a high-performance open-source 3D bioprinter, Sci. Rep. 12 (1) (2022) 22652, https://doi.org/10.1038/s41598-022-26809-4.

[22] C. De Maria, L. Ferrari, F. Montemurro, F. Vozzi, I. Guerrazzi, T. Boland, G. Vozzi, Design and validation of an open-hardware print-head for bioprinting application, Procedia Eng. 110 (2015) 98–105, https://doi.org/10.1016/j.proeng.2015.07.015.

[23] D. Chimene, K.A. Deo, J. Thomas, L. Dahle, C. Mandrona, A.K. Gaharwar, Designing cost-effective open-source multihead 3D bioprinters, GEN biotechnology 1 (4) (2022) 386–400, https://doi.org/10.1089/genbio.2022.0021.

[24] N. Bessler, D. Ogiermann, M.B. Buchholz, A. Santel, J. Heidenreich, R. Ahmmed, B. Brand-Saberi, Nydus One Syringe Extruder (NOSE): a Prusa i3 3D printer conversion for bioprinting applications utilizing the FRESH-method, HardwareX 6 (2019) e00069, https://doi.org/10.1016/j.ohx.2019.e00069.

[25] C.O. Crosby, Open-source extrusion 3D bioprinters: trends and recommendations, Bioprinting (2024) e00336, https://doi.org/10.1016/j.bprint.2024.e00336.

[26] D.J. Cordova, A.A. Rodriguez, S.C. Woodward, C.O. Crosby, The Enderstruder: an accessible open-source syringe extruder compatible with Ender series 3D printers, HardwareX 17 (2024) e00510.

[27] F. Koch, O. Thaden, K. Tröndle, R. Zengerle, S. Zimmermann, P. Koltay, Open-source hybrid 3D-bioprinter for simultaneous printing of thermoplastics and hydrogels, HardwareX 10 (2021) e00230, https://doi.org/10.1016/j.ohx.2021.e00230.

[28] A. Engberg, C. Stelzl, O. Eriksson, P. O'Callaghan, J. Kreuger, An open source extrusion bioprinter based on the E3D motion system and tool changer to enable FRESH and multimaterial bioprinting, Sci. Rep. 11 (1) (2021) 21547, https://doi.org/10.1038/s41598-021-00931-1.

[29] A. Sanz-Garcia, E. Sodupe-Ortega, A. Pernía-Espinoza, T. Shimizu, C. Escobedo-Lucea, A versatile open-source printhead for low-cost 3D microextrusion-based bioprinting, Polymers 12 (10) (2020) 2346, https://doi.org/10.3390/polym12102346.

[30] S. Mohammadi, S. Alessandro, F. Bini, F. Marinozzi, G. Cidonio, Development of a microfluidic-assisted open-source 3D bioprinting system (MOS3S) for the engineering of hierarchical tissues, HardwareX (2024) e00527, https://doi.org/10.1016/j.ohx.2024.e00527.

[31] C. De Maria, G. Vozzi, L. Moroni, Multimaterial, heterogeneous, and multicellular three-dimensional bioprinting, MRS Bull. 42 (8) (2017) 578–584, https://doi.org/10.1557/mrs.2017.165.

[32] S. Micalizzi, L. Russo, C. Giacomelli, F. Montemurro, C. de Maria, M. Nencioni, G. Vozzi, Multimaterial and multiscale scaffold for engineering enthesis organ, International Journal of Bioprinting (2023), https://doi.org/10.18063/ijb.763.

[33] A. De Acutis, C. De Maria, G. Vozzi, Multimaterial and multiscale rapid prototyping of patient-specific scaffold, in: Advances in Science and Technology, 100, 2017, pp. 151–158. http://doi.org/10.4028/www.scientific.net/AST.100.151. Trans Tech Publications Ltd.

[34] Y. Xu, C. Wang, Y. Yang, H. Liu, Z. Xiong, T. Zhang, W. Sun, A multifunctional 3D bioprinting system for construction of complex tissue structure scaffolds: design and application, International Journal of Bioprinting 8 (4) (2022), https://doi.org/10.18063/ijb.v8i4.617.

[35] A. Krige, J. Haluška, U. Rova, P. Christakopoulos, Design and implementation of a low-cost bio-printer modification, allowing for switching between plastic and gel extrusion, HardwareX 9 (2021) e00186, https://doi.org/10.1016/j.ohx.2021.e00186.

[36] M. Lanaro, A. Luu, A. Lightbody-Gee, D. Hedger, S.K. Powell, D.W. Holmes, M. A. Woodruff, Systematic design of an advanced open-source 3D bioprinter for extrusion and electrohydrodynamic-based processes, Int. J. Adv. Des. Manuf. Technol. 113 (2021) 2539–2554, https://doi.org/10.1007/s00170-021-06634-1.

[37] J. Lee, K.E. Kim, S. Bang, I. Noh, C. Lee, A desktop multi-material 3D bio-printing system with open-source hardware and software, Int. J. Precis. Eng. Manuf. 18 (2017) 605–612, https://doi.org/10.1007/s12541-017-0072-x.

[38] T.K. Liu, Y. Pang, Z.Z. Zhou, R. Yao, W. Sun, An integrated cell printing system for the construction of heterogeneous tissue models, Acta Biomater. 95 (2019) 245–257, https://doi.org/10.1016/j.actbio.2019.05.052.

[39] B. Yenilmez, M. Temirel, S. Knowlton, E. Lepowsky, S. Tasoglu, Development and characterization of a low-cost 3D bioprinter, Bioprinting 13 (2019) e00044, https://doi.org/10.1016/j.bprint.2019.e00044.

[40] A. Reizabal, T. Kangur, P.G. Saiz, S. Menke, C. Moser, J. Brugger, S. Luposchainsky, MEWron: an open-source melt electrowriting platform, Addit. Manuf. 71 (2023) 103604, https://doi.org/10.1016/j.addma.2023.103604.

[41] L.X. Phung, T.Q. Ta, V.H. Pham, M.T.H. Nguyen, T. Do, T.K. Nguyen, The development of a modular and open-source multi-head 3D bioprinter for fabricating complex structures, Bioprinting (2024) e00339, https://doi.org/10.1016/j.bprint.2024.e00339.

[42] A.F. Bonatti, G.M. Fortunato, A. Lapomarda, A. De Acutis, C. De Maria, C. V. Brovarone, G. Vozzi, Advanced firmware and hardware for multiscale and multimaterial bioprinting, in: Convegno Nazionale di Bioingegneria, Patron Editore Srl, 2020, pp. 240–243.

[43] H. Gurocak, Industrial Motion Control: Motor Selection, Drives, Controller Tuning, Applications, John Wiley & Sons, 2015.

[44] G.A. Mannella, V. La Carrubba, V. Brucato, Peltier cells as temperature control elements: experimental characterization and modeling, Appl. Therm. Eng. 63 (1) (2014) 234–245, https://doi.org/10.1016/j.applthermaleng.2013.10.069.

[45] S. Kiranlal, V.M. Brathikan, B. Anandh, S. Vikash, A review on electrical and electronics part of 3D printer, in: IOP Conference Series: Materials Science and Engineering, 1228, 2022, March 012007, https://doi.org/10.1088/1757-899X/1228/1/012007. No. 1, IOP Publishing.

[46] T. Staroveški, D. Brezak, T. Udiljak, LINUXCNC–THE enhanced machine controller: application and an overview, Tehnicki vjesnik/Technical Gazette 20 (6) (2013).

[47] G.M. Fortunato, G. Rossi, A.F. Bonatti, A. De Acutis, C. Mendoza-Buenrostro, G. Vozzi, C. De Maria, Robotic platform and path planning algorithm for in situ bioprinting, Bioprinting 22 (2021) e00139, https://doi.org/10.1016/j.bprint.2021.e00139.

[48] A.F. Bonatti, I. Chiesa, G. Vozzi, C. De Maria, Open-source CAD-CAM simulator of the extrusion-based bioprinting process, Bioprinting 24 (2021) e00172, https://doi.org/10.1016/j.bprint.2021.e00172.

[49] A.F. Bonatti, G. Vozzi, C.K. Chua, C. De Maria, A deep learning Quality Control Loop of the extrusion-based bioprinting process, International Journal of Bioprinting 8 (4) (2022), https://doi.org/10.18063/ijb.v8i4.620.

[50] A.F. Bonatti, G. Vozzi, C.K. Chua, C. De Maria, A deep learning approach for error detection and quantification in extrusion-based bioprinting, Mater. Today: Proc. 70 (2022) 131–135, https://doi.org/10.1016/j.matpr.2022.09.006.

[51] S. Vyavahare, S. Kumar, D. Panghal, Experimental study of surface roughness, dimensional accuracy and time of fabrication of parts produced by fused deposition modelling, Rapid Prototyp. J. 26 (9) (2020) 1535–1554.

[52] C.A. Schneider, W.S. Rasband, K.W. Eliceiri, NIH Image to ImageJ: 25 years of image analysis, Nat. Methods 9 (7) (2012) 671–675, https://doi.org/10.1038/nmeth.2089.

[53] A. Lapomarda, E. Pulidori, G. Cerqueni, I. Chiesa, M. De Blasi, M.A. Geven, C. De Maria, Pectin as rheology modifier of a gelatin-based biomaterial ink, Materials 14 (11) (2021) 3109.

[54] A. Lapomarda, G. Cerqueni, M.A. Geven, I. Chiesa, A. De Acutis, M. De Blasi, G. Vozzi, Physicochemical characterization of pectin-gelatin biomaterial formulations for 3D bioprinting, Macromol. Biosci. 21 (9) (2021) 2100168.

[55] G.M. Fortunato, C. De Maria, D. Eglin, T. Serra, G. Vozzi, An ink-jet printed electrical stimulation platform for muscle tissue regeneration, Bioprinting 11 (2018) e00035.

[56] M. Estévez, G. Montalbano, A. Gallo-Cordova, J.G. Ovejero, I. Izquierdo-Barba, B. González, S. Fiorilli, Incorporation of superparamagnetic iron oxide nanoparticles into collagen formulation for 3D electrospun scaffolds, Nanomaterials 12 (2) (2022) 181.